Annual Review of Nuclear and Particle Science

Neutron Star Mergers and Nucleosynthesis of Heavy Elements

F.-K. Thielemann,[1,2] M. Eichler,[3] I.V. Panov,[4,5] and B. Wehmeyer[6]

[1]Department of Physics, University of Basel, CH-4056 Basel, Switzerland; email: f-k.thielemann@unibas.ch

[2]GSI Helmholtzzentrum für Schwerionenforschung, D-64291 Darmstadt, Germany

[3]Institut für Kernphysik, Technische Universität Darmstadt, D-64289 Darmstadt, Germany; email: marius.eichler@theorie.ikp.physik.tu-darmstadt.de

[4]Institute for Theoretical and Experimental Physics, National Research Center Kurchatov Institute, Moscow 123098, Russia; email: panov_iv@itep.ru

[5]Sternberg Astronomical Institute, M.V. Lomonosov State University, Moscow 119234, Russia

[6]Department of Physics, North Carolina State University, Raleigh, North Carolina 27695-8202

Annu. Rev. Nucl. Part. Sci. 2017. 67:253–74

First published as a Review in Advance on August 7, 2017

The *Annual Review of Nuclear and Particle Science* is online at nucl.annualreviews.org

https://doi.org/10.1146/annurev-nucl-101916-123246

Keywords

compact binary/neutron star mergers, r-process, nuclear properties far from stability, chemical evolution of galaxies

Abstract

The existence of neutron star mergers has been supported since the discovery of the binary pulsar and the observation of its orbital energy loss, consistent with General Relativity. They are considered nucleosynthesis sites of the rapid neutron-capture process (r-process), which is responsible for creating approximately half of all heavy elements beyond Fe and is the only source of elements beyond Pb and Bi. Detailed nucleosynthesis calculations based on the decompression of neutron star matter are consistent with solar r-process abundances of heavy nuclei. Neutron star mergers have also been identified with short-duration γ-ray bursts via their IR afterglow. The high neutron densities in ejected matter permit a violent r-process, leading to fission cycling of the heaviest nuclei in regions far from (nuclear) stability. Uncertainties in several nuclear properties affect the abundance distributions. The modeling of astrophysical events also depends on the hydrodynamic treatment, the occurrence of a neutrino wind after the merger and before the

possible emergence of a black hole, and the properties of black hole accretion disks. We discuss the effect of nuclear and modeling uncertainties and conclude that binary compact mergers are probably a (or the) dominant site of the production of r-process nuclei in our Galaxy.

Contents

1. INTRODUCTION

Neutron stars, whose existence was postulated shortly after the discovery of the neutron, were predicted to be the ultimate fate of massive stars, ending in supernova events (1). Their existence was proven in the 1960s after the first observations of pulsars (2). We now have extensive knowledge of the distribution of neutron star masses and the underlying equation of state (e.g., 3–5); the most precise determinations exist for binary systems. Shortly after the discovery of the binary pulsar (6), which loses energy as predicted by General Relativity, it was found that the system would merge in 10^8 years. This finding led to the prediction that neutron stars or neutron star–black hole mergers would eject rapid neutron-capture process (r-process) nuclei (7–9). This prediction was followed by a detailed analysis of possible abundance distributions (10). Such mergers were later predicted to be accompanied by neutrino bursts and γ-ray bursts (GRBs) (11). The first, and later more precise, estimates of the mass ejection from neutron star mergers in a Newtonian approximation followed (12–15), together with the first detailed nucleosynthesis predictions (16).

More recently, extensive investigations have been undertaken with respect to nucleosynthesis predictions (17–37). New approaches have gone beyond a Newtonian treatment, ranging from conformally flat to fully relativistic treatments (e.g., 22, 24, 26, 38–42), and have included the role of magnetic fields (43). Modern simulations consider not only the composition of the dynamical ejecta but also the composition of the neutrino wind (along the poles), in which matter is ejected from the combined (initially rotationally stabilized) hot neutron star (e.g., 20, 26, 29, 31, 37, 41, 42, 44, 45), up to the point of black hole formation if the maximum neutron star mass is exceeded (46), followed

by the ejection of matter from (viscous) black hole accretion disks. The outflow of black hole accretion disks has been investigated in detail (e.g., 27, 35, 47–51), and the effect of neutrino conversion via matter–neutrino resonances has been analyzed with respect to a possible impact on nucleosynthesis (52–56); for a good overview of all these components, including jet formation and ejection, see Reference 57. Neutron star–black hole mergers have also been investigated (e.g., 20, 58–63).

Such nucleosynthesis predictions have been extensively tested with respect to nuclear uncertainties due to masses far from stability, β decays, fission barriers, and fission fragment distributions (e.g., 23, 28, 30, 32, 51, 64, 65). The effect of the nuclear equation of state has been studied as well (e.g., 22, 27, 39–41, 66, 67).

An extensive literature relates these events to short-duration GRBs and/or macronovae as electromagnetic counterparts (e.g., 25, 46, 63, 68–75a). This issue was the topic of Fernández & Metzger's (76) review in a recent volume of this journal, and we refer to that article herein. Although these objects are important as strong sources of gravitational wave emission (77), underpinning the importance of multimessenger observations, this review focuses on the ejected nucleosynthesis composition. The nucleosynthesis is constrained by solar r-process abundances and whether they can be reproduced by compact object mergers; by observations of low-metallicity stars, which are affected by the occurrence frequency as a function of time in early galactic evolution; and finally by information from individual events, which relate to the observed light curve and spectra (here the nucleosynthetic composition connects via its effect on opacities to the electromagnetic signal).

This review is organized as follows. Section 2 covers observational constraints, Section 3 describes the required thermodynamic conditions and neutron richness of the ejecta, and Section 4 presents a detailed discussion of nucleosynthesis results from compact object mergers. Section 5 returns to issues in Galactic evolution and discusses whether compact binary mergers can match observations in the early Galaxy. Section 6 presents our conclusions.

2. OBSERVATIONAL EVIDENCE FOR r-PROCESS NUCLEOSYNTHESIS

2.1. Solar r-Process Abundances and Patterns in Low-Metallicity Stars

One interesting aspect to be tested relates to whether mergers lead to a robust r-process environment that produces heavy r-elements (at least, those with $A \geq 130$) in proportions similar to solar abundances (**Figure 1**) (78–80). However, there are variations in the contributions of lighter elements with $Z \leq 50$ (81). Could this be due to variations in the production site, or are different production sites required? A fraction of old metal-poor halo stars shows a wide variety of abundance signatures, including r-elements such as Eu (e.g., 82–84), which may indicate a different weaker neutron-capture source, perhaps a fraction of regular supernovae (85, 86). Finally, note that not in all low-metallicity star observations do Th and U appear in solar proportions (or with appropriate abundances due to their decay since production). Since this initial discovery (87), several such abundance patterns have been observed, so far all in extremely metal-poor stars. This could indicate changes in the r-process strength for the same r-process sites.

2.2. Early Galactic Evolution

As mixing of ejecta into the interstellar medium is not instantaneous, there will be local inhomogeneities after individual nucleosynthesis events. Mixing occurs via the propagation of a Sedov–Taylor blast wave through interstellar matter until the (kinetic) explosion energy is expended, working against the ram pressure of the surrounding medium. For a standard explosion energy of $E = 10^{51}$ erg (a unit known as 1 Bethe, or 1 foe, an acronym based on 10 to the power of fifty-one ergs) and typical densities of the interstellar medium, this results in mixing with approximately

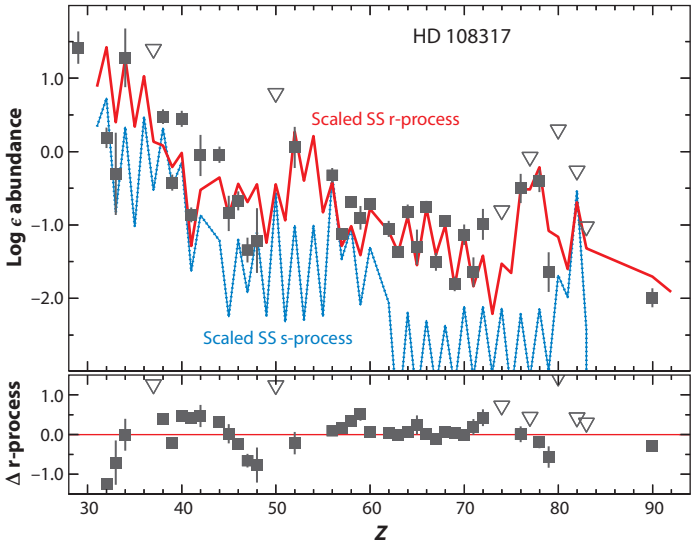

Figure 1

The observed abundances of a typical low-metallicity star (HD 108317) unveil a clear r-process (and not an s-process) pattern, exactly as found in the Solar System (SS), at least for elements with $Z \geq 40$. Modified with permission from Reference 78. Copyright AAS.

a few 10^4 $M_\odot$. Mixing can also occur via more macroscopic effects, like spiral arm movements (timescales of 10^8 years), and turbulent mixing (possibly with timescales as low as 10^7 years). These macroscopic mixing effects can smooth spatial abundance gradients. If they are neglected or unimportant for the regions and timescales of interest, the composition in regions directly affected by the explosive blast wave of a specific event will be maintained until many other events from specific stellar sources and explosions overlap spatially. When this situation is attained, it will lead to an integrated average of ejecta compositions. Thus, although we expect an average value of, for example, [Eu/Fe] to occur in late galactic evolution, rare events will lead to large variations at low metallicities, depending on whether a rare nearby strong r-process source polluted the environment or was absent.

Neutron star mergers have high predicted ejecta masses of the order of a few times 10^{-3} to 10^{-2} $M_\odot$ of overall r-process matter in their dynamic ejecta (see also Section 4.3 for a comparable contribution from black hole accretion disk winds). They are rarer than regular core-collapse supernovae (CCSNe) by a factor of 100 to 1,000 (91, 92). Such event rates are consistent with population synthesis studies (93) and with (inhomogeneous) chemical evolution calculations (62, 94–100). The latter can follow local variations of abundances due to specific contributions by individual explosions. The scatter of r-process elements (e.g., Eu) compared with Fe at low metallicities covers more than two orders of magnitude (**Figure 2**), indicating production sites with negligible Fe production (101) and a low event rate combined with high ejecta masses in order to explain solar abundances. The low event rate causes the effect that for [Eu/Fe] the approach to an average ratio occurs only in the interval $-2 \leq$ [Fe/H] ≤ -1. The approach to an average ratio as a function of [Fe/H] is shifted for [Mg/Fe] to a lower metallicity range, $-4 \leq$ [Fe/H] ≤ -3, due to the much higher CCSN rate (responsible for Mg as well as Fe) in comparison to neutron star mergers.

Dwarf galaxies, especially ultrafaint dwarf galaxies, are polluted only by a few events (102–105) or, in extreme cases, a single event, as observed in, for example, Reticulum II (106, 107). These observations require events with high r-process ejecta masses, consistent with the conclusions

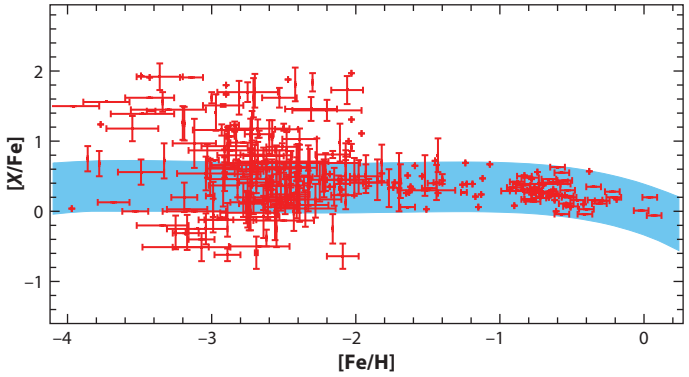

Figure 2

Ratios of [Mg/Fe] (blue uncertainty range, indicating 95% of observations) and [Eu/Fe] (individual stellar observations shown as red error bars) as a function of metallicity [Fe/H] for stars in our Galaxy (88–90). $[X/Y]$ stands for $\log_{10}[(X/Y)/(X/Y)_\odot]$, specifically, [Mg/Fe] = 0 or [Fe/H] = 0 for solar ratios, −1 for one-tenth of the solar ratio, and so forth. Mg shows a relatively flat behavior up to [Fe/H] ≤ -1, similar to other α elements such as O, Mg, Si, S, Ar, Ca, and Ti, decreasing to solar values at [Fe/H]= 0. This behavior is explained by the early contributions of core-collapse supernovae before type Ia supernovae set in. The real scatter is probably smaller than indicated by the blue region, which represents a collection of many observations from different telescopes, different observers, and different analysis techniques. By contrast, the scatter of Eu/Fe is larger than two orders of magnitude at low metallicities, indicating production sites with a low event rate, and thus takes longer to arrive at average values only in the interval $-2 \leq$ [Fe/H] ≤ -1. These average values are observed for α elements (with a core-collapse supernova origin) in the range $-4 \leq$ [Fe/H] ≤ -3. Modified from Reference 88.

presented above for low-metallicity stars in the Milky Way. The Milky Way might have evolved from an assembly of initially individual dwarf galaxies in which the efficiency and rate of star formation varied in these early components before the present Galaxy emerged (99, 108, 109).

2.3. Short-Duration Gamma-Ray Bursts and Macronovae

Compared with the overall constraints discussed in the previous subsection (e.g., how to reproduce the solar r-process abundance pattern), indications for individual events are harder to obtain. Low-metallicity stars can serve this purpose to some extent, as they might have been polluted by only a single nucleosynthesis event. A clearer constraint is based on direct observations of a single event in order to test whether theoretical predictions for an r-process are underpinned by observational proofs of these objects. Neutron star mergers have been identified with short-duration GRBs or macronovae via the light curves and spectra of their electromagnetic counterparts. These are not yet proof of a detailed abundance pattern, but the existing observations can only be understood through the opacities of (very) heavy elements (e.g., 63, 69, 72, 110–112). The radioactive energy emitted from heavy unstable nuclear species, together with its thermalization efficiency, sets the luminosity budget and is therefore crucial for predicting macronova light curves. In modeling the macronova accompanying GRB 130603B, estimates for the mass ejection could be made (75) in that event. This study showed that late-time macronova light curves can be significantly affected by α decay from trans-Pb isotopes, which could be used as a diagnostic test for more detailed ejecta abundances. We refer the reader to the recent review by Fernández & Metzger (76), which discusses this topic in great detail. The main message is that only with opacities of very heavy elements are the light curves and spectra of these events explainable; in other words, short-duration GRBs produce these heavy elements in sizable amounts. Although the observations integrate

over many elements (including radioactive elements), a detailed abundance pattern cannot be determined, but there is hope that future investigations will identify specific features (75).

2.4. Recent Radioactive Additions to the Solar System

Whereas the above discussion considers rare strong r-process events in the early Galaxy, there exist other observations suggesting similar events in recent history. Long-lived radioactive species can act as witnesses to recent additions to the Solar System, depending on their half-lives. For a review of the signature of radioactive isotopes that existed in the early Solar System, see, for example, Reference 113.

Two isotopes have recently been utilized to perform such measurements in deep-sea sediments. The first, ^{60}Fe, has a half-life of 2.6×10^6 years and can indicate recent additions from events occurring up to several million years ago. ^{60}Fe is produced during the evolution and explosion of massive stars (leading to supernovae) (114, 115). It is found in deep-sea sediments that incorporated stellar debris from a nearby explosion approximately two million years ago (116–118). The second isotope, ^{244}Pu, has a half-life of 8.1×10^7 years and would give rise to a collection of many such supernova events. If the strong r-process took place in every CCSN from massive stars, then approximately 10^{-4}–10^{-5} $M_\odot$ of r-process matter would need to be ejected per event in order to explain the present-day solar abundances. The recent detection of ^{244}Pu (119) is lower than would be expected from such predictions by two orders of magnitude, suggesting that actinide nucleosynthesis is very rare (permitting substantial decay since the last nearby event) and that supernovae did not contribute significantly to it in the solar neighborhood during the past few hundred million years. Thus, in addition to the inherent problems faced by (regular) CCSN models in setting the conditions required for a strong r-process—which also produces the actinides—these observational constraints from nearby events challenge the idea that regular CCSNe are a source of main r-process contributions. A recent careful study of the origin of the strong r-process with continuous accretion of interstellar dust grains into the inner Solar System (34) concluded that the experimental observations (119) provide evidence for an r-process origin from a rare event, such as a neutron star merger. This would explain the existence of ^{244}Pu in the very early Solar System, as well as the low levels of more recently deposited ^{244}Pu isotopes observed in deep-sea sediments over the past few hundred million years.

3. CONDITIONS FOR MAKING THE HEAVIEST ELEMENTS

Many potential sites for the r-process have been suggested. These include regular CCSNe; neutrino-induced processes in the outer shells of massive stars; ejecta from compact binary mergers; and a special class of CCSNe, termed magnetohydrodynamic or MHD-jet supernovae, with fast rotation, high magnetic fields, and neutron-rich jet ejecta along the poles. In all of these cases, the production of r-process nuclei occurs in a two-stage process: (*a*) an initial explosive burning at high temperatures until charged-particle freeze-out during expansion, with a high neutron-to-seed ratio, followed by (*b*) the rapid capture of neutrons on the seed nuclei, producing the heaviest nuclei.

3.1. Explosive Burning and Charged-Particle Freeze-Out

In the first stage of the production of r-process nuclei, matter experiences explosive burning at high temperatures and is heated to conditions that permit so-called nuclear-statistical equilibrium (NSE), which indicates full chemical equilibrium among all of the involved nuclear reactions. At density ρ and temperature T, nucleus i (with neutron number N_i, proton number Z_i, and mass

number $A_i = Z_i + N_i$) has abundance Y_i, expressed in terms of the abundances of free neutrons Y_n and protons Y_p:

$$Y_i = G_i(\rho N_A)^{A_i-1}\frac{A_i^{3/2}}{2^{A_i}}\left(\frac{2\pi\hbar^2}{m_u k_b T}\right)^{3/2(A_i-1)}\exp(B_i/k_b T)Y_n^{N_i}Y_p^{Z_i}. \quad 1.$$

Here, G_i is the partition function of nucleus i, k_b is the Boltzmann constant, N_A is Avogadro's number, m_u is the nuclear mass unit, and B_i is the nuclear binding energy of the nucleus. β decays, electron captures, and neutrino interactions change the overall proton-to-nucleon ratio, $Y_e = \sum Z_i Y_i / \sum A_i Y_i$ (the denominator is the sum of all mass fractions and therefore is equal to unity), and occur on longer timescales than do particle captures and photodisintegrations. They are not in equilibrium and have to be followed explicitly. Thus, as a function of time, NSE follows the corresponding densities $\rho(t)$, temperatures $T(t)$, and $Y_e(t)$, leading to two equations based on total mass conservation and the existing Y_e:

$$\sum_{i>n,p} A_i Y_i = Y_n + Y_p + \sum_{i>n,p}(Z_i + N_i)Y_i(\rho, T, Y_n, Y_p) = 1, \quad 2.$$

$$\sum_i Z_i Y_i = Y_p + \sum_{i>p} Z_i Y_i(\rho, T, Y_n, Y_p) = Y_e. \quad 3.$$

In general, very high densities favor large nuclei, due to the high power of ρ^{A_i-1}, and very high temperatures favor light nuclei, due to $(k_b T)^{-3/2(A_i-1)}$. In the intermediate regime, $\exp(B_i/k_b T)$ favors tightly bound nuclei, with the highest binding energies in the mass range $A = 50$–60 of the Fe group, depending on the given Y_e. The width of the composition distribution is determined by the temperature. Thus, in the first stage of this scenario, high temperatures cause nuclei to (photo)disintegrate into neutrons, protons, and α particles due to the energy distribution of the blackbody photon gas. During the subsequent cooling and expansion of matter, a buildup of heavier nuclei sets in, still governed by the trend of keeping matter in NSE. However, the buildup of nuclei beyond He is hampered by the need for reaction sequences involving highly unstable ^{8}Be (e.g., $\alpha+\alpha+\alpha \rightarrow {}^{12}$C or $\alpha+\alpha+n \rightarrow {}^{9}$Be), which are strongly dependent on the density of matter. The first part of these reaction sequences involves a chemical equilibrium for $\alpha + \alpha \leftrightarrow {}^8$Be, which is strongly shifted to the left side of the reaction equation because of the half-life of ^{8}Be ($\tau_{1/2} = 6.7 \times 10^{-17}$ s). Reasonable amounts of ^{8}Be, which permit the second stage of these reactions via an α particle or neutron capture, can be built up only for high densities. The reaction rates for the combined reactions have a quadratic dependence on density, as opposed to the linear density dependence in regular fusion reactions. Therefore, for low densities the NSE cannot be maintained, and after further cooling and freezing out of charged-particle reactions, an overabundance of α particles (He) remains, permitting only a (much) smaller fraction of heavier elements to be formed than in NSE for the intermediate regime (determined by the binding energies of nuclei). This result, also called α-rich freeze-out (of charged-particle reactions), causes (*a*) the abundance of nuclei heavier than He to be (strongly) reduced in comparison to their NSE abundances and (*b*) the abundance maximum of the (fewer) heavy nuclei to be shifted (via final α captures) to heavier nuclei in comparison to NSE. Although this maximum would normally be around Fe and Ni (the highest binding energies) with $A = 50$–60, it may be up to $A \sim 90$.

In hot environments, the total entropy is dominated by the blackbody photon gas (radiation) and is proportional to T^3/ρ (120, 121); in other words, the combination of high temperatures and low densities leads to high entropies. Thus, high entropies cause α-rich freeze-out, and (depending on the entropy) only small amounts of Fe-group elements are produced—essentially all of the matter that passed through the bottleneck beyond He (**Figure 3*a***).

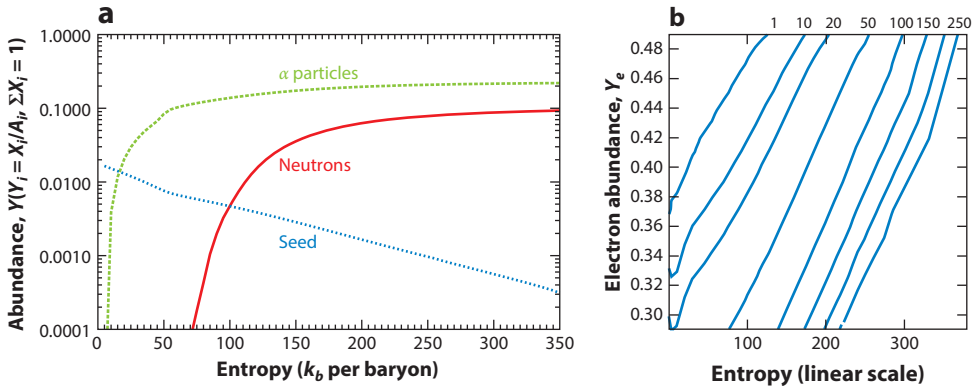

Figure 3

(*a*) Abundances of neutrons (Y_n), ^{4}He (α particles; Y_α), and so-called seed nuclei (Y_{seed}) in the mass range $50 \leq A \leq 100$, resulting from the charged-particle freeze-out of explosive burning, as a function of entropy in the explosively expanding plasma (122). The ratio of neutrons to seed nuclei (Y_n/Y_{seed}) increases with entropy. The number of neutrons per seed nucleus determines whether the heaviest elements (actinides) can be produced in a strong r-process, which requires $A_{\text{seed}} + (Y_n/Y_{\text{seed}}) \geq 230$. Panel *a* modified from Reference 122. (*b*) Y_n/Y_{seed} (*contour lines*) resulting from the expansion of hot plasmas in explosive burning as a function of electron abundance (Y_e) and entropy (measured in k_b per baryon). A strong r-process that produces actinides with $Y_n/Y_{\text{seed}} = 150$ requires, for moderate Y_e values of approximately 0.45, entropies beyond 250. Panel *b* modified from Reference 123.

The calculation for **Figure 3*a***, performed with an expansion timescale equivalent to a free-fall for those conditions and a Y_e value of 0.45, shows how with increasing entropies the α mass fraction ($X_\alpha = 4Y_\alpha$) approaches unity and the number of heavier elements (which would provide the seed nuclei for a later r-process) approaches zero. Similarly, in the Big Bang, extremely high entropies permitted essentially only elements up to He, as well as tiny amounts of Li. In contrast to the Big Bang, which was proton rich, the conditions chosen here ($Y_e = 0.45$) are slightly neutron rich, leading predominantly to He and free neutrons at high entropies. The small number of heavier nuclei following charged-particle freeze-out (in the mass range of $A = 50$–100), depending on the entropy or α-richness of the freeze-out, can then act as seed nuclei for capture of the free neutrons. As a prerequisite for an r-process producing nuclei as heavy as the actinides and starting from nuclei with $A = 50$–100, a neutron-to-seed ratio of approximately 150 is required. This ratio is depicted as a contour plot and as a function of entropy and Y_e in **Figure 3*b*** (123).

A different behavior occurs for lower entropies, namely the expansion of relatively cold and/or high-density matter, as it exists in ejected neutron star matter. At such low entropies, the contour lines for the constant neutron-to-seed ratios shown in **Figure 3*b*** would bend and become flat; the resulting ratio would essentially be only a function of Y_e. In order to obtain a neutron-to-seed ratio of 150, a Y_e value on the order of 0.1 would be required.

3.2. Neutron Captures in the r-Process

Once freeze-out of charged-particle reactions occurs and a full chemical equilibrium (NSE) can no longer be maintained, the simplified approach described in Section 3.1 ceases to be valid. Therefore, all nuclear reactions have to be followed via extended nuclear reaction networks. There

exist three types of terms in the reaction network equations, which predict the time derivatives of nuclear abundances Y_i as a function of all other abundances entering reactions that produce or destroy Y_i:

$$\frac{\mathrm{d}Y_i}{\mathrm{d}t} = \sum_j P^i_j \, \lambda_j Y_j + \sum_{j,k} P^i_{j,k} \, \rho N_\mathrm{A} < j,k > Y_j Y_k + \sum_{j,k,l} P^i_{j,k,l} \, \rho^2 N^2_\mathrm{A} < j,k,l > Y_j Y_k Y_l. \quad 4.$$

One has to sum over all of the reaction partners given by the different summation indices. The *P*s include an integer (positive or negative) factor N^i, which describes whether (and how often) nucleus i is created or destroyed in this reaction, as well as correction factors that avoid multiple counting in case two or three identical reaction partners are involved. The λs stand for decay rates (including decays, photodisintegrations, electron captures, and neutrino-induced reactions), $<j,k>$ denotes the thermal average of the product of the reaction cross section σ and the relative velocity v of reactions between nuclei j and k, and $<j,k,l>$ includes a similar expression for three-body reactions (124). For a survey of computational methods to solve nuclear networks, see References 125 and 126. The abundances Y_i are related to number densities $n_i = \rho N_\mathrm{A} Y_i$ and mass fractions of the corresponding nuclei via $X_i = A_i Y_i$. Data repositories of the experimental and theoretical reaction rates that are required as input for Equation 4 can be found elsewhere (see Related Resources). A more detailed discussion of modeling nucleosynthesis processes is provided in Reference 114.

As charged-particle reactions are frozen at approximately 3×10^9 K, the isotopic chains are connected only by β decays (unless fission sets in, repopulating lighter nuclei from fission fragments). High neutron densities make the timescales for neutron capture much faster than those for β decays and can produce nuclei with neutron separation energies S_n of 2 MeV and lower. This is the energy gained (i.e., the Q value) when a neutron is captured on nucleus $A-1$, and/or the photon energy required to release a neutron from nucleus A via photodisintegration. At the neutron drip line, S_n decreases to zero; in other words, for high neutron densities, leading to vanishing values of S_n, the r-process proceeds close to the neutron drip line. For temperatures around 10^9 K, (γ, n) photodisintegrations can still be very active for such small-reaction S_n values, as only temperatures related to $\sim 30\,kT \geq S_n$ are required for these reverse reactions to dominate. As both reaction directions are faster than the process timescales (and β decays), chemical equilibrium can set in between the neutron captures and photodisintegrations. In this case, the complete chemical equilibrium (or NSE)—discussed at the beginning of this subsection—splits into many (quasi-)equilibrium clusters, each of which represents an isotopic chain of heavy nuclei. The abundance distribution of each isotopic chain follows the ratio of the two neighboring isotopes,

$$\frac{Y(Z,A+1)}{Y(Z,A)} = n_n \frac{G(Z,A+1)}{2G(Z,A)} \left[\frac{A+1}{A}\right]^{3/2} \left[\frac{2\pi\hbar^2}{m_u kT}\right]^{3/2} \exp[S_n(A+1)/kT], \quad 5.$$

where the partition functions G describe the thermal population of the excited states; the nuclear mass unit is m_u; and the neutron separation (or binding) energy of nucleus $(Z, A+1)$, $S_n(A+1)$, is the neutron capture Q value of nucleus (Z, A). The abundance ratios depend only on $n_n = \rho N_\mathrm{A} Y_n$, T, and S_n. S_n introduces the dependence on nuclear masses, namely a nuclear mass model for these very neutron-rich unstable nuclei. Under the assumption of a $(n,\gamma) \rightleftharpoons (\gamma, n)$ equilibrium, no detailed knowledge of neutron capture cross sections is needed.

One fact that can be easily deduced—given that $Y(A+1)/Y(A)$ rises with increasing distance from stability, is close to one at the abundance maximum of the isotopic chain, and finally decreases—is that the abundance maxima in each isotopic chain are determined only by the

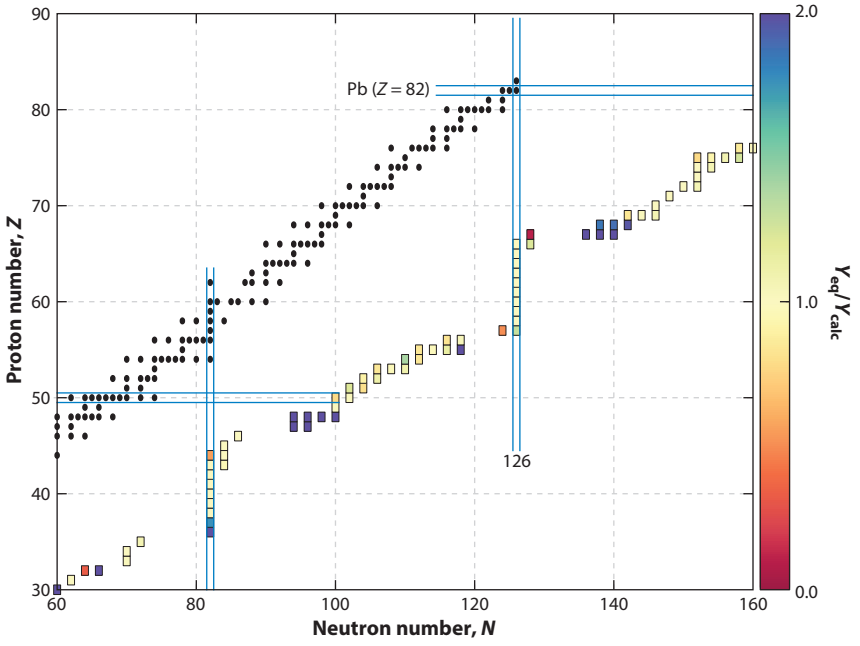

Figure 4

The line of stability (*black circles*) and the r-process path, resulting from a neutron star merger environment (30). The position of the path follows from a chemical equilibrium between neutron captures and photodisintegrations in each isotopic chain [(n,γ)–(γ,n) equilibrium], determined by neutron number density, temperature, and the nuclear mass model utilized [here, the Finite Range Droplet Model (FRDM) (129)]. The present calculations were performed with a complete nuclear network containing more than 3,000 nuclei. The colors along the path indicate how well the full network calculations follow such an (n,γ)–(γ,n) equilibrium. The full calculations agree with this equilibrium approach within a factor of two along the r-process path, here with an approximate neutron separation energy of 2 MeV, which continues to the heaviest nuclei. Only in the final phase of the process, when neutron number densities and temperatures decline, does such an equilibrium freeze out, and some final changes of the abundance pattern can occur due to continuing neutron captures. Modified from Reference 30.

neutron number density n_n and the temperature T. If we approximate $Y(Z, A{+}1)/Y(Z, A)$ by 1 at the maximum, consider that the ratios of partition functions of neighboring nuclei and $(A+1)/A$ are also close to unity, and keep temperature and density constant, the neutron separation energy S_n has to be the same for the abundance maxima in all isotopic chains (**Figure 4**). Note that all current nucleosynthesis calculations have been obtained from full solutions of extended reaction networks determined by Equation 4. However, the use of Equations 1–3 and 5 can act as a test of whether such equilibria exist and can aid our understanding of the numerical results. **Figure 4** displays just such a test for the conditions in neutron star mergers (30).

3.3. The Influence of Nuclear Properties

Figure 4 shows the r-process path, corresponding to a contour line of approximately 2 MeV for the Finite Range Droplet Model (FRDM) (129), at a location far from the stability line. As the speed along the r-process path is determined by β decays, which are longer closer to stability, abundance maxima will occur at the top end of the kinks in the r-process path at neutron shell

closures $N = 50, 82$, and 126. The mass numbers $A_{\text{path}}(N_{\text{shell}})$, where the path passes neutron shell closures, are smaller than the mass numbers $A_{\text{stable}}(N_{\text{shell}})$ for stable nuclei at the same neutron shell closure. (This feature remains after β decay back to stability at the end of the process.) In environments with sufficiently high neutron densities, the r-process continues toward extremely heavy nuclei and finally encounters the neutron shell closure $N = 184$, where fission plays a dominant role. **Figure 5** (also based on simulations in Reference 30) shows the regions of the nuclear chart where fission dominates and where the fission fragments are located.

The following section applies the general mechanism of and nuclear input into an r-process to neutron star merger environments. The influence of nuclear uncertainties should be analyzed, independently of the conditions encountered, and how they affect the results obtained should be determined. Recent tests involving mass models, β decay half-lives, and fission fragment distributions (23, 30, 32, 51, 64) have utilized a variety of mass models, β decays, and fission properties (17, 23, 127–136) and have analyzed the effect of neutrinos (e.g., 28, 29, 31); the most advanced treatments of neutrino interactions in matter with medium corrections can be found in References 137 and 138. Finally, tests for neutrino flavor conversion via matter–neutrino resonances have been performed (e.g., 55, 56).

4. THE r-PROCESS IN COMPACT BINARY MERGERS

A brief overview of the history of neutron star–black hole or binary neutron star mergers, especially their role with respect to nucleosynthesis contributions, is provided in Section 1, above. In this section, we discuss the main results from recent research (e.g., 18–37, 41, 42, 51, 67) including simulations that consider not only the composition of the dynamical ejecta but also the composition of the neutrino wind (along the poles), where matter is ejected from the combined (initially rotationally stabilized) hot neutron star up to the point of black hole formation, followed by the ejection of matter from (viscous) black hole accretion disks. The following subsections discuss each of these topics in turn.

4.1. Dynamical Ejecta

One result of early investigations that studied only dynamical ejecta (i.e., matter "thrown out" dynamically after the merger of two compact objects with a very low Y_e) was that abundances below the second r-process peak (at $A = 130$) would originate only from fission products. Thus, lighter r-process elements beyond the Fe group have already experienced neutron capture and are depleted in the final result. In addition, especially for Newtonian calculations, material tended to be perhaps too neutron rich. This tendency led to large numbers of very heavy nuclei prone to fission, which remain at high abundances up to the final stages of the simulations. Although the initial conditions of the r-process seem ideally suited to reproduce the second and third r-process peaks and their positions (**Figure 4**), during the final phase the fission of the heaviest nuclei produces large numbers of neutrons. If this occurs during or after the freeze-out from (n, γ)–(γ, n) equilibrium, these neutrons can modify the overall abundance pattern inherited from the earlier equilibrium, shifting the third r-process peak. Several tests based on the latest knowledge of nuclear physics far from stability have been performed and can improve the overall abundance pattern. These tests relate to mass model properties such as fission probabilities and fragment distributions (**Figure 6**) as well as β decay half-lives (135, 136), which speed up the production of the heaviest nuclei and cause the final phase of fission to set in earlier with respect to the freeze-out; moreover, the release of fewer late neutrons has less of an effect on the pattern of the third r-process peak (**Figure 6*a*,*b***) (30).

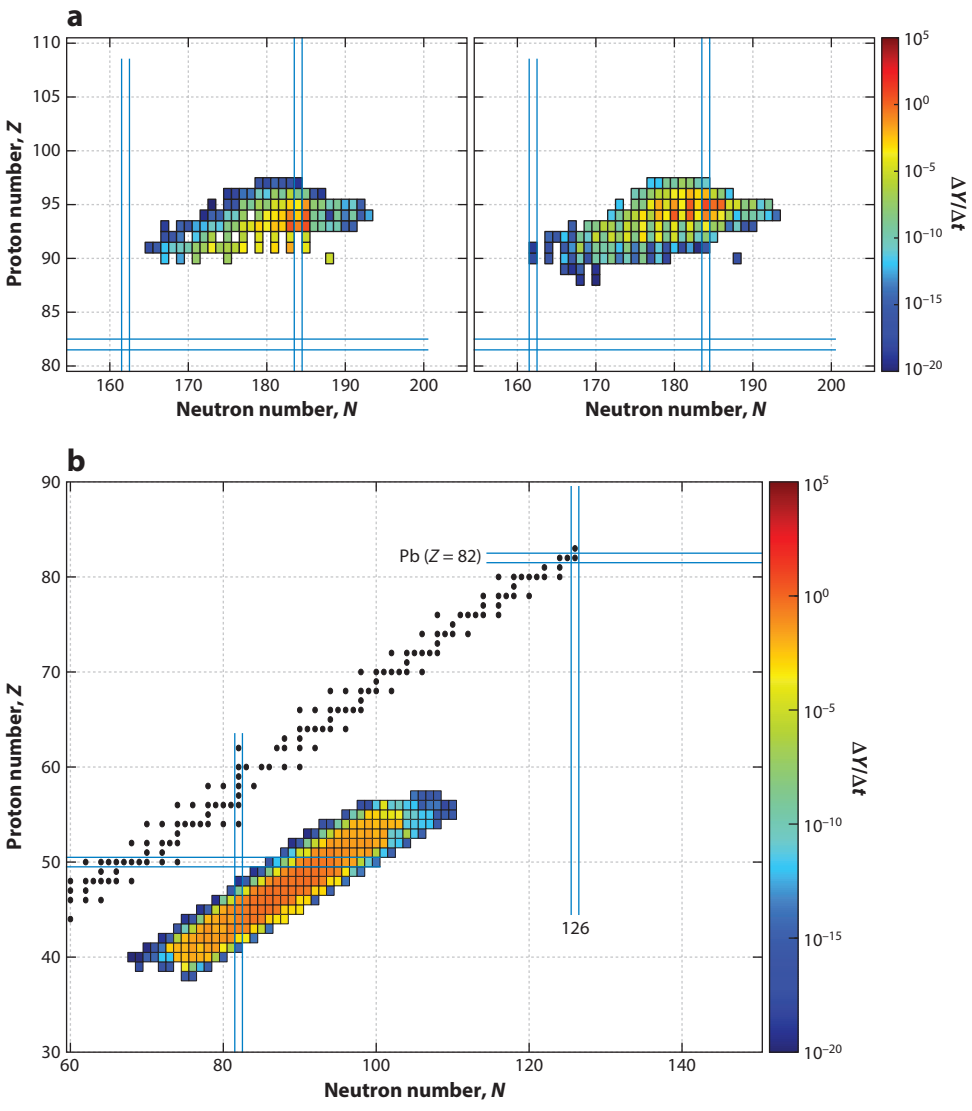

Figure 5

Time derivatives (*color-coded*) of nuclear abundances Y during an r-process simulation (30), due to (*a*) the destruction via neutron-induced and β-delayed fission (127) and (*b*) the production of fission fragments (128). The latter are produced in a broad distribution in the mass number range $A = 115$–155. Modified from Reference 30.

4.2. Neutrino Winds and the Effect of Neutrino Spectra

A neutrino wind (similar to that in CCSNe) from a hot, very massive combination of two neutron stars will contribute to the nucleosynthesis of these events after the dynamic ejecta discussed above. This hot central object, supported by high temperatures and rotation, will not collapse into a black hole immediately, and the surrounding matter will experience the radiation of neutrinos

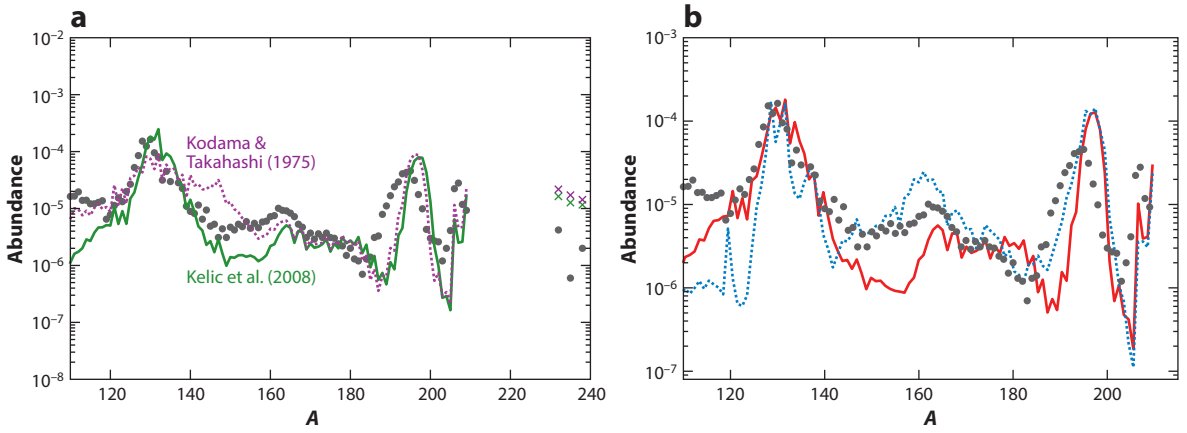

Figure 6

(*a*) r-Process abundances, compared with solar values (*gray dots*), resulting from neutron star merger simulations (30), using β decay half-lives (134) together with a relatively old set (*purple line*) (139) and a modern set (128) of fragment distributions of fissioning nuclei. In both cases, the third r-process peak seems to shift in the final phases, driven by neutron capture of the released fission neutrons. (*b*) Same as in panel *a*, but with recent β decay half-life predictions (*dashed blue line*) (135) in comparison to the older set (red line corresponding to the green line in panel *a*). Faster β decays for heavy nuclei speed up the r-process and deliver (also in the final phases) nuclei that are prone to fission at an earlier time. Thus, the late release of fission neutrons occurs earlier, largely before the freeze-out from (n,γ)–(γ,n) equilibrium. Therefore, final neutron captures after freeze-out, which can distort this distribution, are strongly reduced, as shown by a comparison between the two panels. Modified from Reference 30.

and antineutrinos, changing Y_e by the following reactions:

$$\nu_e + n \quad \rightarrow \quad p + e^-, \qquad 6.$$

$$\bar{\nu}_e + p \quad \rightarrow \quad n + e^+. \qquad 7.$$

These reactions render matter neutron rich only if the average antineutrino energy $\langle \epsilon_{\bar{\nu}_e} \rangle$ is higher than the average neutrino energy $\langle \epsilon_{\nu_e} \rangle$ by four times the neutron–proton mass difference Δ for similar (electron) neutrino L_{ν_e} and antineutrino $L_{\bar{\nu}_e}$ luminosities. This fact, first pointed out in Reference 140, approaches, due to neutrino and antineutrino captures with the given luminosities and average energies, the following equilibrium value of the proton-to-nucleon ratio:

$$Y_e = \left[1 + \frac{L_{\bar{\nu}_e}(\langle \epsilon_{\bar{\nu}_e} \rangle - 2\Delta + 1.2\Delta^2/\langle \epsilon_{\bar{\nu}_e} \rangle)}{L_{\nu_e}(\langle \epsilon_{\nu_e} \rangle + 2\Delta + 1.2\Delta^2/\langle \epsilon_{\nu_e} \rangle)}\right]^{-1}. \qquad 8.$$

For further details and in-medium corrections for neutrons and protons in comparison to their treatment as free particles, see References 137 and 138. In most cases, the energetically favorable first reaction wins, changing Y_e from the initial (neutron-rich) conditions to values closer to 0.5, leading only to a weak r-process and producing matter below the second r-process peak. The first estimate of this outcome was presented in Reference 25. More detailed results are available (**Figure 7**) (29, 31, 36, 37, 45).

A related factor also affects the dynamical ejecta. Several of the simulations discussed above were performed with Newtonian physics—that is, nonrelativistically. For neutron stars, and especially the resulting black holes, the role of General Relativity is important and leads to deeper gravitational potentials plus higher temperatures experienced by the matter involved. As a result, electron–positron pairs, positron captures on neutrons, and the effect of neutrino radiation even

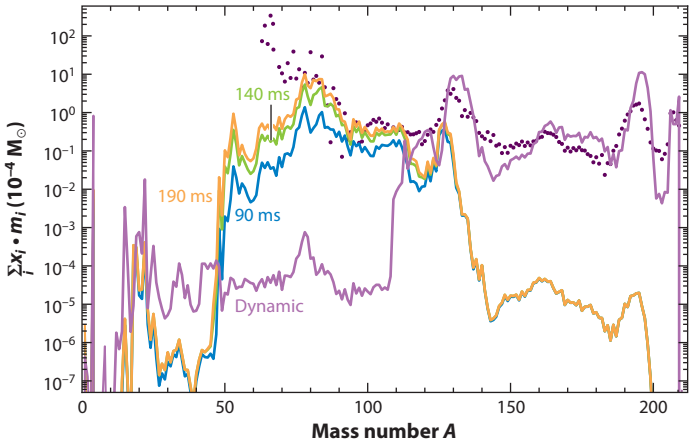

Figure 7

The neutrino wind contribution to neutron star merger ejecta, which depends on the delay time (in milliseconds) between the merger and black hole formation (31). The dynamic ejecta from Reference 20 are shown for comparison. The neutrino wind, ejected dominantly in polar regions, contributes nuclei with $A < 130$, due to the effect of the neutrinos on Y_e. Modified from Reference 31.

for the dynamical ejecta become more important. The result is an increase in Y_e from a value of 0.05 or lower in pure neutron star matter to a value around 0.1–0.15 (26, 28, 41, 42) for dynamical ejecta, and even higher values in the neutrino wind. As a result, less fission cycling occurs, producing less late emission of fission neutrons and therefore avoiding some of the deficiencies of the abundance patterns discussed above with respect to **Figure 6** (also observed in the dynamic ejecta component of **Figure 7**).

Possible changes in Y_e can also be obtained through the modification of neutrino and antineutrino spectra due to neutrino flavor conversion. Several tests to verify such neutrino conversions via matter–neutrino resonances have been performed (52–56). The more-complicated geometry of a disk environment, in comparison to CCSNe, has until now permitted only single-angle approximations, which might limit the accuracy of current results. However, existing investigations clearly point to the possibility that Y_e, and thus the resulting nucleosynthesis, can be affected.

4.3. Black Hole Accretion Disks

After the stabilizing effect of the rotation of the massive merged object fades, a central black hole (being beyond the maximum mass of cold neutron stars) will usually form. Such environments, which represent the ultimate fate of neutron star mergers, require investigation into disk winds from black hole accretion disks, which had initially been tested as sites of heavy-element nucleosynthesis (47–49). Detailed simulations for such sites resulting from mergers of binary compact objects have recently been performed (27, 35, 51, 76), leading to predictions of comparable masses in dynamical ejecta and disk outflows [with a slight dominance of dynamical ejecta for neutron star mergers and the opposite effect for neutron star–black hole mergers (76)]. The latest results for disk outflows (51) are displayed in **Figure 8**, which shows the integrated ejecta of all tracer particles. The figure demonstrates that outflows alone can produce a robust abundance pattern around the second r-process peak at $A = 130$, with significant production of $A \leq 130$ nuclei. In most of the simulations, the disk outflows also reach the third peak at $A = 195$.

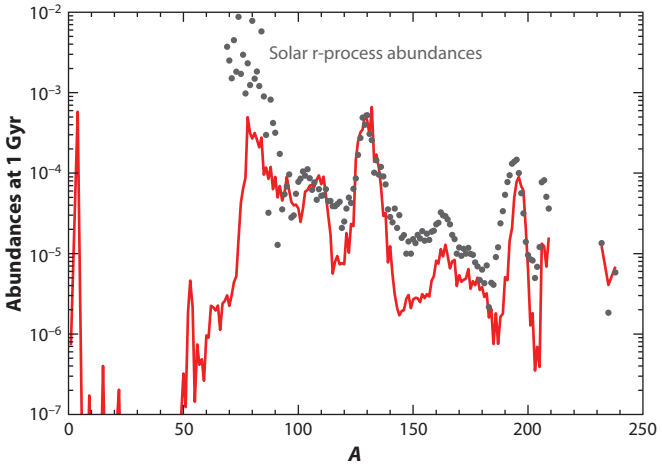

Figure 8

r-Process abundances, compared with solar values (*gray dots*), resulting from black hole accretion disk simulations (51), using a black hole mass of 3 $M_\odot$, a disk mass of 0.03 $M_\odot$, an initial Y_e of 0.1, entropy per baryon of $8k_b$, an α parameter of the viscous disk of 0.03, and a vanishing black hole spin. Modified from Reference 51 with permission from Oxford University Press on behalf of the Royal Astronomical Society.

The detailed results depend on the disk viscosity, the initial mass or entropy of the torus, the black hole spin, and (of course) the nuclear physics input. In particular, the production of heavy ($A = 195$) nuclei is affected by the uncertainties of these disk properties. However, such a deficit can be easily counterbalanced by the dynamic ejecta, as the total nucleosynthesis of the merger includes the components of the dynamic ejecta, the neutrino wind, and the black hole accretion disk.

5. A NEED FOR AN r-PROCESS CONTRIBUTION FROM MASSIVE SINGLE STARS?

The previous sections show that compact binary mergers can in all cases reproduce the heavy solar r-process abundances (if not most of them); that they can explain short-duration GRBs and related macronova events; that they are rare, consistent with low-metallicity observations and findings from deep-sea sediments; and that, in combination with ejecta masses and occurrence frequency, they can also explain the total amount of solar r-process matter (within the given uncertainties). There seems to be only one caveat. A binary neutron star merger requires two prior supernova events (which produce the two neutron stars and, e.g., Fe ejecta) plus the gravitational wave–driven inspiral in order to result in a merger. There is a time delay between the Fe-producing supernovae and r-process ejection that can shift the appearance of a typical r-process tracer such as Eu to higher metallicities [Fe/H] (**Figure 9**) (94, 95, 98). Such results rely to some extent on the coalescence times (and their distribution) in binary systems, the local star formation rate, and the amount of mixing of the ejecta with the surrounding interstellar medium (33). The results shown in **Figure 9** are based on mixing with the surrounding medium via a Sedov–Taylor blast wave (typically of order 5×10^4 $M_\odot$) and with varying coalescence times. The latter seem not to solve the problem of reproducing the [Eu/Fe] ratio in low-metallicity stars.

However, there exist other galactic mixing events (e.g., turbulent mixing) on varying timescales that could blur the picture. Relatively low resolutions in global galaxy evolution models with

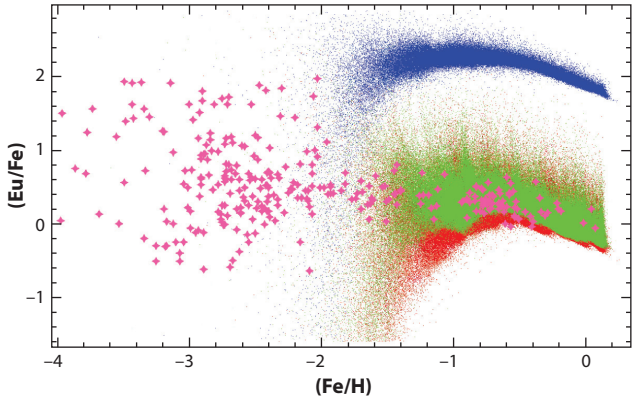

Figure 9

Influence of the coalescence timescale and neutron star merger probability on Eu abundances in galactic chemical evolution. The magenta stars represent observations. The red dots correspond to model star abundances as in Reference 94. The coalescence timescale is 10^8 years with a typical probability consistent with population synthesis (98). The green dots illustrate the effect on the abundances if the coalescence timescale is shorter (around 10^6 years). The blue dots represent the change in abundance if the probability of neutron star mergers is increased. Within this treatment of galactic chemical evolution, none of these options would permit a fit with observations of low-metallicity stars in the metallicity range $-4 \leq [\text{Fe/H}] \leq -2.5$. Modified from Reference 98.

smooth particle hydrodynamics simulations (96, 97) can wash out the behavior shown in **Figure 9** at low metallicities, but a high-resolution run recovers it (see figure 4 of Reference 96). The history of the local star formation rate can differ, if the galaxy formed from small substructures that merge at late times in galactic evolution (99, 108). Such aspects still need to be resolved. Alternatively, a rare class of CCSNe, exploding earlier in galactic evolution with a negligible time delay to star formation, could contribute at low metallicities. Early suggestions that so-called electron-capture supernovae in the range 8–10 $M_\odot$ (141–144) would be able to produce a strong r-process were never confirmed, and they would not correspond to rare events. However, other objects driven by strong magnetic fields and fast rotation (possibly approximately 1% or less of all CCSNe), leaving behind 10^{15}-G neutron stars (magnetars), might play a significant role. Such magnetorotational supernovae show similar characteristics in the amount of r-process ejecta and possibly occurrence frequency as neutron star mergers, but—because these objects result from massive single stars—they do not experience the delay of binary evolution (85, 86, 145–149). This might be interesting with respect to the subdivision of short-duration GRBs into those with a delay and those that directly follow the star formation rate (73).

Such magnetorotational supernovae, which are rare events and prolific in r-process ejecta, could enter galactic evolution at the lowest metallicities with a scatter similar to that of binary compact mergers. Existing observations show evidence for the occurrence of MHD-jet supernovae [magnetars (150)]. In inhomogeneous Galactic evolution simulations without extended turbulent mixing, a superposition of MHD-jet supernovae and neutron star mergers can match observations over the whole Galactic evolution, from the lowest metallicities (i.e., in the early Galaxy), up to the present. Note that there exist uncertainties in mixing processes, star formation rates, and so forth that will affect behavior at the lowest metallicities. However, depending on rotation frequency, magnetic fields, and the impact of neutrino heating in comparison to the strength of magnetic

fields, the strength of the r-process can vary (85, 86), whereas neutron star mergers seem to predict a robust and unchangeable abundance pattern. At low metallicities, there exist observations with a Eu/U ratio that changes somewhat, indicating the extent to which the production of actinides is robustly coupled to Eu. Several events with a regular r-process pattern but changing amounts of actinides have been observed at metallicities around [Fe/H] $= -3$. Thus, such variations, which are not expected from compact binary mergers, might indicate an effect of MHD-jet supernovae at low metallicities. It is reasonable to expect that, at low metallicities, MHD-jet supernovae are more frequent than in the present Galaxy. Low-metallicity stars have less wind and mass loss, and therefore less angular momentum loss, providing more promising initial conditions at the onset of collapse for these events.

6. CONCLUSIONS

This review summarizes our present knowledge of r-process conditions in compact binary mergers, their ability to produce a solar abundance pattern, their role in Galactic evolution and recent additions to the Solar System, and finally some open questions that still need to be solved or complemented by other sites:

1. Extended sets of simulations have shown that compact binary mergers are prolific sites of r-process nucleosynthesis, leading to approximately a few 10^{-3} to 10^{-2} $M_\odot$ of ejected r-process matter in the dynamic ejecta. When all components are included—from the early dynamic ejecta directly after the merger, over ejecta caused by the neutrino wind during the phase of a hot central merged object, and finally (in case the latter becomes a black hole) the late disk wind from a viscous black hole accretion disk—the combined ejecta contain not only the heaviest r-process nuclei but also a significant amount of the standard solar r-process abundances for nuclei with $A < 130$. The sizable production of r-process matter (with comparable masses from dynamic ejecta and disk outflows; see figure 4 of Reference 76) requires these events to be rare if they are responsible for reproducing all Galactic r-process material (see also figure 2 of Reference 63).
2. Radioactive tracers such as ^{244}Pu and ^{60}Fe are found in deep-sea sediments. The production of ^{60}Fe in frequent events, related to regular CCSNe and/or electron capture supernovae, is supported by the latest contribution dating back approximately two million years. By contrast, the amount of ^{244}Pu found in these sediments is lower than expected by a factor of approximately 100, if such quasi-continuous production is assumed. This points to substantial decay since the last addition and, consequently, to much rarer events.
3. Observations of the lowest-metallicity stars in our Galaxy and (ultrafaint) dwarf galaxies show substantial "pollution" by r-process elements, indicating a production site with a low event rate and a consistently high amount of r-process ejecta in order to explain solar abundances. The large scatter of Eu/Fe (Eu is an r-process element, and Fe stems from CCSNe at low metallicities) observed in the earliest stars of the Galaxy supports the idea that the nucleosynthesis products of regular CCSNe and these rare events (producing substantial amounts of Eu and probably negligible amounts of Fe) are not yet well mixed in the interstellar medium.
4. Neutron star mergers (or neutron star–black hole mergers) are related to short-duration GRBs and their electromagnetic counterparts (macronovae). These macronovae (i.e., the electromagnetic afterglow) can be explained only if the opacity of ejected matter is dominated by heavy elements. Population synthesis supports the idea that these events are very

rare (probably approximately one one-hundredth to one one-thousandth of the CCSN frequency).

5. The major open question is whether products of the neutron star merger r-process can explain the observations of r-process elements already observed at metallicities of [Fe/H] ≤ -3. Because the supernovae that produce the neutron stars of a merger already lead to a substantial floor of Fe—that is, enhance [Fe/H]—only substantial turbulent mixing of interstellar medium matter in the early Galaxy could reproduce these observations in Galactic chemical evolution calculations. A way out of this conclusion could be that neutron star kicks, emerging at birth in supernova explosions, would remove the binary neutron star system from the debris of the supernova explosion and place it into a medium with low Fe pollution.
6. There exist observational indications of 10^{15}-G neutron stars. A rare class of CCSNe driven by a magnetorotational mechanism could lead to such neutron stars with immense magnetic fields and produce r-process matter ejected in polar jets. However, predictions from stellar evolution about the distribution of magnetic fields and rotation rates before core collapse are needed in order to understand the initial conditions that could lead to such events. The role of the magnetorotational instability during the collapse and explosion phase has to be investigated.
7. Such objects, which probably also have a low event rate of the order of one one-hundredth to one one-thousandth that of regular CCSNe, could avoid the problems of the neutron star merger scenario at low metallicities, as they are related to massive single stars and do not experience any delay in comparison to regular CCSNe.
8. Independently of these points related to astrophysical observations and the modeling of complex astrophysical sites, the final test of whether the detailed abundance pattern of heavy elements can be reproduced relies on a deep knowledge and understanding of the nuclear properties that enter such calculations, including masses far from stability over weak interactions; the determination of β decay properties and electron/positron captures on nucleons and nuclei; neutrino properties affecting their interaction with matter; and fission barriers and fission fragment distributions. In addition, the equation of state utilized at the highest densities and temperatures sets the conditions for such environments.

DISCLOSURE STATEMENT

The authors are not aware of any affiliations, memberships, funding, or financial holdings that may be perceived as affecting the objectivity of this review.

ACKNOWLEDGMENTS

We thank all our collaborators and everybody with whom we have had enlightening discussions on the topics of neutron star mergers and r-process nucleosynthesis. These include Almudena Arcones, Gabriele Cescutti, Cristina Chiappini, John Cowan, Khalil Farouqi, Maik Frensel, Brad Gibson, Samuel Giuliani, Yuhri Ishimaru, Thomas Janka, Oliver Just, Roger Käppeli, Oleg Korobkin, Karl-Ludwig Kratz, Karlheinz Langanke, Jim Lattimer, Andreas Lohs, Lucio Mayer, Matthias Liebendörfer, Tomislav Marketin, Dirk Martin, Gabriel Martínez-Pinedo, Francesca Matteucci, Gail McLaughlin, Nobuya Nishimura, Francesco Pannarale, Albino Perego, Marco Pignatari, Tsvi Piran, Thomas Rauscher, Stephan Rosswog, Chris Sneden, Rebecca Surman, Tomoya Takiwaki, Cristina Volpe, Shinja Wanajo, Christian Winteler, Meng-Ru Wu, and many others. This research was supported by the Swiss National Science Foundation (via a regular research grant and a SCOPES grant for collaborations with Eastern Europe), an Advanced

European Research Council Grant from the European Commission (FISH), and the Russian Science Foundation (project number 16-12-10519).

NOTE ADDED IN PROOF

While this article was going to press, there were rumors and indications that the LIGO/VIRGO consortium had observed gravitational waves from a neutron star merger. This observation, apparently associated with a short-duration GRB and an electromagnetic counterpart, provides evidence that nucleosynthesis of very heavy elements has taken place. If this observation is confirmed, the combination of all three aspects would have been seen for the very first time, thus providing essential constraints on the working of neutron star mergers and their nucleosynthesis.

LITERATURE CITED

1. Baade W, Zwicky F. *Phys. Rev.* 46:76 (1934)
2. Hewish A, Okoye SE. *Nature* 207:59 (1965)
3. Özel F, Psaltis D, Narayan R, Santos Villarreal A. *Astrophys. J.* 757:55 (2012)
4. Hebeler K, Lattimer JM, Pethick CJ, Schwenk A. *Astrophys. J.* 773:11 (2013)
5. Oertel M, Hempel M, Klähn T, Typel S. *Rev. Mod. Phys.* 89:015007 (2017)
6. Hulse RA, Taylor JH. *Astrophys. J.* 195:L51 (1975)
7. Lattimer JM, Schramm DN. *Astrophys. J.* 192:L145 (1974)
8. Lattimer JM, Schramm DN. *Astrophys. J.* 210:549 (1976)
9. Symbalisty E, Schramm DN. *Astrophys. J.* 22:143 (1982)
10. Meyer BS, Schramm DN. In *Origin and Distribution of the Elements*, ed. GJ Mathews, p. 610. Singapore: World Sci. (1988)
11. Eichler D, Livio M, Piran T, Schramm DN. *Nature* 340:126 (1989)
12. Davies MB, Benz W, Piran T, Thielemann F-K. *Astrophys. J.* 431:742 (1994)
13. Ruffert M, Janka H-T, Schäfer G. *Astron. Astrophys.* 311:532 (1996)
14. Rosswog S, et al. *Astron. Astrophys.* 341:499 (1999)
15. Rosswog S, Davies MB, Thielemann F-K, Piran T. *Astron. Astrophys.* 360:171 (2000)
16. Freiburghaus C, Rosswog S, Thielemann F-K. *Astrophys. J.* 525:L121 (1999)
17. Panov IV, Thielemann F-K. *Astron. Lett.* 30:647 (2004)
18. Panov IV, Korneev IY, Thielemann F-K. *Astron. Lett.* 34:189 (2008)
19. Goriely S, Bauswein A, Janka H-T. *Astrophys. J.* 738:L32 (2011)
20. Korobkin O, Rosswog S, Arcones A, Winteler C. *Mon. Not. R. Astron. Soc.* 426:1940 (2012)
21. Panov IV, Korneev IY, Lutostansky YS, Thielemann F-K. *Phys. At. Nucl.* 76:88 (2013)
22. Bauswein A, Goriely S, Janka H-T. *Astrophys. J.* 773:78 (2013)
23. Goriely S, et al. *Phys. Rev. Lett.* 111:242502 (2013)
24. Hotokezaka K, Kyutoku K, Shibata M. *Phys. Rev. D* 87:044001 (2013)
25. Rosswog S, et al. *Mon. Not. R. Astron. Soc.* 439:744 (2014)
26. Wanajo S, et al. *Astrophys. J.* 789:L39 (2014)
27. Just O, et al. *Mon. Not. R. Astron. Soc.* 448:541 (2015)
28. Goriely S, et al. *Mon. Not. R. Astron. Soc.* 452:3894 (2015)
29. Perego A, et al. *Mon. Not. R. Astron. Soc.* 443:3134 (2014)
30. Eichler M, et al. *Astrophys. J.* 808:30 (2015)
31. Martin D, et al. *Astrophys. J.* 813:2 (2015)
32. Mendoza-Temis JJ, et al. *Phys. Rev. C* 92:055805 (2015)
33. Ramirez-Ruiz E, et al. *Astrophys. J.* 802:L22 (2015)
34. Hotokezaka K, Piran T, Paul M. *Nat. Phys.* 11:1042 (2015)
35. Just O, et al. *Astrophys. J.* 816:L30 (2016)
36. Radice D, et al. *Mon. Not. R. Astron. Soc.* 460:3255 (2016)

37. Roberts LF, et al. *Mon. Not. R. Astron. Soc.* 464:3907 (2017)
38. Oechslin R, Rosswog S, Thielemann F-K. *Phys. Rev. D* 65:103005 (2002)
39. Oechslin R, Uryū K, Poghosyan G, Thielemann F-K. *Mon. Not. R. Astron. Soc.* 349:1469 (2004)
40. Oechslin R, Janka H-T, Marek A. *Astron. Astrophys.* 467:395 (2007)
41. Sekiguchi Y, Kiuchi K, Kyutoku K, Shibata M. *Phys. Rev. D* 91:064059 (2015)
42. Sekiguchi Y, et al. *Phys. Rev. D* 93:124046 (2016)
43. Kiuchi K, et al. *Phys. Rev. D* 92:124034 (2015)
44. Dessart L, et al. *Astrophys. J.* 690:1681 (2009)
45. Lehner L, et al. *Class. Quantum Gravity* 33:184002 (2016)
46. Metzger BD, Fernández R. *Mon. Not. R. Astron. Soc.* 441:3444 (2014)
47. Surman R, McLaughlin GC, Hix WR. *Astrophys. J.* 643:1057 (2006)
48. Surman R, et al. *Astrophys. J.* 679:L117 (2008)
49. Surman R, et al. *J. Phys. G* 41:044006 (2014)
50. Fernández R, Kasen D, Metzger BD, Quataert E. *Mon. Not. R. Astron. Soc.* 446:750 (2015)
51. Wu MR, Fernández R, Martínez-Pinedo G, Metzger BD. *Mon. Not. R. Astron. Soc.* 463:2323 (2016)
52. Malkus A, Kneller JP, McLaughlin GC, Surman R. *Phys. Rev. D* 86:085015 (2012)
53. Foucart F, et al. *Phys. Rev. D* 91:124021 (2015)
54. Malkus A, McLaughlin GC, Surman R. *Phys. Rev. D* 93:045021 (2016)
55. Zhu YL, Perego A, McLaughlin GC. *Phys. Rev. D* 94:105006 (2016)
56. Frensel M, Wu MR, Volpe C, Perego A. *Phys. Rev. D* 95:023011 (2017)
57. Hotokezaka K, Piran T. *Mon. Not. R. Astron. Soc.* 450:1430 (2015)
58. Rosswog S. *Astrophys. J.* 634:1202 (2005)
59. Wanajo S, Janka H-T. *Astrophys. J.* 746:180 (2012)
60. Kyutoku K, Ioka K, Shibata M. *Phys. Rev. D* 88:041503 (2013)
61. Foucart F, et al. *Phys. Rev. D* 90:024026 (2014)
62. Mennekens N, Vanbeveren D. *Astron. Astrophys.* 564:A134 (2014)
63. Rosswog S, et al. *Class. Quantum Gravity* 34:104001 (2017)
64. Mumpower MR, Surman R, McLaughlin GC, Aprahamian A. *Prog. Part. Nucl. Phys.* 86:86 (2016)
65. Shibagaki S, et al. *Astrophys. J.* 816:79 (2016)
66. Bauswein A, Stergioulas N, Janka H-T. *Phys. Rev. D* 90:023002 (2014)
67. Bauswein A, Stergioulas N, Janka H-T. *Eur. Phys. J. A* 52:56 (2016)
68. Li LX, Paczyński B. *Astrophys. J.* 507:L59 (1998)
69. Tanvir NR, et al. *Nature* 500:547 (2013)
70. Tanaka M, Hotokezaka K. *Astrophys. J.* 775:113 (2013)
71. Kasen D, Badnell NR, Barnes J. *Astrophys. J.* 774:25 (2013)
72. Grossman D, Korobkin O, Rosswog S, Piran T. *Mon. Not. R. Astron. Soc.* 439:757 (2014)
73. Wanderman D, Piran T. *Mon. Not. R. Astron. Soc.* 448:3026 (2015)
74. Hotokezaka K, et al. *Mon. Not. R. Astron. Soc.* 459:35 (2016)
75. Barnes J, Kasen D, Wu MR, Martínez-Pinedo G. *Astrophys. J.* 829:110 (2016)
75a. Metzger BD. *Living Rev. Relativ.* 20:3 (2017)
76. Fernández R, Metzger BD. *Annu. Rev. Nucl. Part. Sci.* 66:23 (2016)
77. Abbott BP, et al. *Phys. Rev. Lett.* 116:131103 (2016)
78. Roederer IU, et al. *Astrophys. J.* 791:32 (2014)
79. Sneden C, Cowan JJ, Gallino R. *Annu. Rev. Astron. Astrophys.* 46:241 (2008)
80. Roederer IU, et al. *Astrophys. J. Suppl.* 203:27 (2012)
81. Qian YZ, Wasserburg GJ. *Phys. Rep.* 442:237 (2007)
82. Honda S, et al. *Astrophys. J.* 643:1180 (2006)
83. Hansen CJ, Montes F, Arcones A. *Astrophys. J.* 797:123 (2014)
84. Roederer IU. *Astrophys. J.* 835:23 (2017)
85. Nishimura N, Takiwaki T, Thielemann F-K. *Astrophys. J.* 810:109 (2015)
86. Nishimura N, et al. *Astrophys. J.* 836:L21 (2017)
87. Cayrel R, et al. *Nature* 409:691 (2001)
88. Thielemann F-K. *Nat. Phys.* 11:993 (2015)

89. Suda T, et al. *Publ. Astron. Soc. Jpn.* 60:1159 (2008)
90. Suda T, et al. *Mon. Not. R. Astron. Soc.* 412:843 (2011)
91. Matteucci F, et al. *Mon. Not. R. Astron. Soc.* 447:326 (2015)
92. Macias P, Ramirez-Ruiz E. arXiv:1609.04826 [astro-ph] (2016)
93. Chruslinska M, Belczynski K, Bulik T, Gladysz W. *Acta Astron.* 67:37 (2017)
94. Argast D, Samland M, Thielemann F-K, Qian Y-Z. *Astron. Astrophys.* 416:997 (2004)
95. Cescutti G, et al. *Astron. Astrophys.* 577:A139 (2015)
96. van de Voort F, et al. *Mon. Not. R. Astron. Soc.* 447:140 (2015)
97. Shen S, et al. *Astrophys. J.* 807:115 (2015)
98. Wehmeyer B, Pignatari M, Thielemann F-K. *Mon. Not. R. Astron. Soc.* 452:1970 (2015)
99. Hirai Y, et al. *Astrophys. J.* 814:41 (2015)
100. Mennekens N, Vanbeveren D. *Astron. Astrophys.* 589:A64 (2016)
101. Cowan JJ, et al. *Astrophys. J.* 627:238 (2005)
102. Cohen JG, Huang W. *Astrophys. J.* 701:1053 (2009)
103. Jablonka P, et al. *Astron. Astrophys.* 583:A67 (2015)
104. Simon JD, et al. *Astrophys. J.* 802:93 (2015)
105. Tsujimoto T, Nishimura N. *Astrophys. J.* 811:L10 (2015)
106. Ji AP, Frebel A, Chiti A, Simon JD. *Nature* 531:610 (2016)
107. Ji AP, Frebel A, Simon JD, Chiti A. *Astrophys. J.* 830:93 (2016)
108. Ishimaru Y, Wanajo S, Prantzos N. *Astrophys. J.* 804:L35 (2015)
109. Beniamini P, Hotokezaka K, Piran T. *Astrophys. J.* 832:149 (2016)
110. Metzger BD, et al. *Mon. Not. R. Astron. Soc.* 406:2650 (2010)
111. Berger E, Fong W, Chornock R. *Astrophys. J.* 774:L23 (2013)
112. Yang B, et al. *Nat. Commun.* 6:7323 (2015)
113. Davis AM, McKeegan KD. In *Treatise on Geochemistry*, vol. 1: *Meteorites and Cosmochemical Processes*, ed. AM Davis, p. 361. Amsterdam: Elsevier (2014)
114. Thielemann F-K, Hirschi R, Liebendörfer M, Diehl R. In *Lecture Notes in Physics*, vol. 812: *Astronomy with Radioactivites*, ed. R Diehl, DH Hartmann, N Prantzos, p. 3. Berlin: Springer (2011)
115. Wanajo S, Janka H-T, Müller B. *Astrophys. J.* 774:L6 (2013)
116. Knie K, et al. *Phys. Rev. Lett.* 93:171103 (2004)
117. Wallner A, et al. *Nature* 532:69 (2016)
118. Fimiani L, et al. *Phys. Rev. Lett.* 116:151104 (2016)
119. Wallner A, et al. *Nat. Commun.* 6:5956 (2015)
120. Woosley SE, Hoffman RD. *Astrophys. J.* 395:202 (1992)
121. Roberts LF, Woosley SE, Hoffman RD. *Astrophys. J.* 722:954 (2010)
122. Farouqi K, et al. *Astrophys. J.* 712:1359 (2010)
123. Freiburghaus C, et al. *Astrophys. J.* 516:381 (1999)
124. Nomoto K, Thielemann F-K, Miyaji S. *Astron. Astrophys.* 149:239 (1985)
125. Hix WR, Thielemann F-K. *J. Comput. Appl. Math.* 109:321 (1999)
126. Timmes FX. *Astrophys. J. Suppl.* 124:241 (1999)
127. Panov IV, et al. *Astron. Astrophys.* 513:A61 (2010)
128. Kelic A, Ricciardi MV, Schmidt KH. In *Dynamical Aspects of Nuclear Fission*, ed. J Kliman, MG Itkis, S Gmuca, p. 203. Singapore: World Sci. (2008)
129. Möller P, Nix JR, Myers WD, Swiatecki WJ. *At. Data Nucl. Data Tables* 59:185 (1995)
130. Duflo J, Zuker AP. *Phys. Rev. C* 52:R23 (1995)
131. Möller P, Myers WD, Sagawa H, Yoshida S. *Phys. Rev. Lett.* 108:052501 (2012)
132. Goriely S, Chamel N, Pearson JM. *Phys. Rev. C* 88:024308 (2013)
133. Wang N, Liu M. *J. Phys. Conf. Ser.* 420:012057 (2013)
134. Möller P, Pfeiffer B, Kratz KL. *Phys. Rev. C* 67:055802 (2003)
135. Marketin T, Huther L, Martínez-Pinedo G. *Phys. Rev. C* 93:025805 (2016)
136. Panov IV, Lutostansky YS, Thielemann F-K. *Nucl. Phys. A* 947:1 (2016)
137. Martínez-Pinedo G, Fischer T, Lohs A, Huther L. *Phys. Rev. Lett.* 109:251104 (2012)
138. Roberts LF, Reddy S, Shen G. *Phys. Rev. C* 86:065803 (2012)

139. Kodama T, Takahashi K. *Nucl. Phys. A* 239:489 (1975)
140. Qian YZ, Woosley SE. *Astrophys. J.* 471:331 (1996)
141. Kitaura FS, Janka H-T, Hillebrandt W. *Astron. Astrophys.* 450:345 (2006)
142. Janka H-T, Müller B, Kitaura FS, Buras R. *Astron. Astrophys.* 485:199 (2008)
143. Wanajo S, et al. *Astrophys. J.* 695:208 (2009)
144. Wanajo S, Janka H-T, Müller B. *Astrophys. J.* 726:L15 (2011)
145. Fujimoto Si, Nishimura N, Hashimoto M. *Astrophys. J.* 680:1350 (2008)
146. Ono M, et al. *Prog. Theor. Phys.* 128:741 (2012)
147. Winteler C, et al. *Astrophys. J.* 750:L22 (2012)
148. Mösta P, et al. *Astrophys. J.* 785:L29 (2014)
149. Mösta P, et al. *Nature* 528:376 (2015)
150. Greiner J, et al. *Nature* 523:189 (2015)

RELATED RESOURCES

1. Reaclib Database. **https://groups.nscl.msu.edu/jina/reaclib/db/**
2. NON-SMOKER Database. **https://nucastro.org/reaclib.html**
3. Karlsruhe Astrophysical Database of Nucleosynthesis in Stars. **http://www.kadonis.org/**
4. Brussels Nuclear Library for Astrophysics Applications. **http://www.astro.ulb.ac.be/pmwiki/Brusslib/HomePage**

Annual Review of Nuclear and Particle Science

Volume 67, 2017

Contents

Errata

An online log of corrections to *Annual Review of Nuclear and Particle Science* articles may be found at http://www.annualreviews.org/errata/nucl